Article

Structure

Ligand Binding Mechanism in Steroid Receptors: From Conserved Plasticity to Differential Evolutionary Constraints

Graphical Abstract

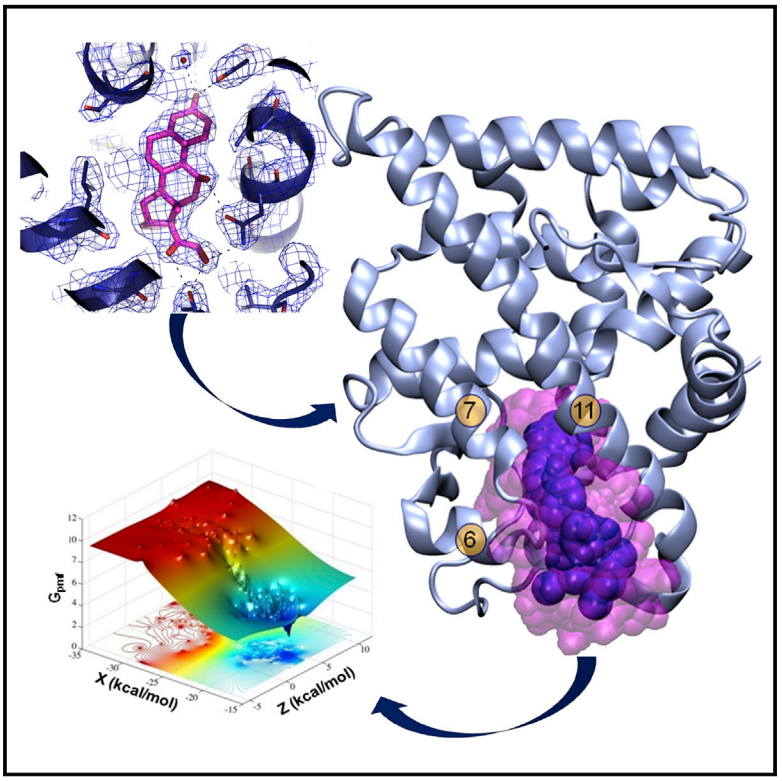

Highlights

- X-Ray structures of MR and GR reveal a conserved plasticity near helices 6 and 7
- Ligand binding simulations provide a functional role to the observed plasticity
- Residence time measurements correlate with the proposed binding mechanism
- Differences in receptor blueprints promote differential evolutionary constraints

Authors

Karl Edman, Ali Hosseini, Magnus K. Bjursell, ..., Matti Lepistö, Anders C. Hogner, Victor Guallar

Correspondence

anders.hogner@astrazeneca.com (A.C.H.), victor.guallar@bsc.es (V.G.), karl.edman@astrazeneca.com (K.E.)

In Brief

Edman et al. combined X-ray crystallography, computational simulations, and residence time measurements to uncover the ligand entry and exit processes of steroid hormone receptors. Subsequent bioinformatics analyses confirmed that differences in the details of the ligand entry mechanism lead to differential selection pressure across the receptor family.

Edman et al., 2015, Structure *23*, 2280–2290
December 1, 2015
http://dx.doi.org/10.1016/j.str.2015.09.012

CellPress

Structure
Article

Ligand Binding Mechanism in Steroid Receptors: From Conserved Plasticity to Differential Evolutionary Constraints

Karl Edman,[1,*] Ali Hosseini,[2] Magnus K. Bjursell,[3] Anna Aagaard,[1] Lisa Wissler,[1] Anders Gunnarsson,[1] Tim Kaminski,[1] Christian Köhler,[4] Stefan Bäckström,[1] Tina J. Jensen,[4] Anders Cavallin,[4] Ulla Karlsson,[1] Ewa Nilsson,[1] Daniel Lecina,[2] Ryoji Takahashi,[2] Christoph Grebner,[5] Stefan Geschwindner,[1] Matti Lepistö,[4] Anders C. Hogner,[5,*] and Victor Guallar[2,6,*]

[1]Discovery Sciences, AstraZeneca, Mölndal, Pepparedsleden 1, 43183 Mölndal, Sweden

[2]Joint BSC-CRG-IRB Research Program in Computational Biology, Barcelona Supercomputing Center, Jordi Girona 29, 08034 Barcelona, Spain

[3]R&D Information, AstraZeneca, Pepparedsleden 1, 43183 Mölndal, Sweden

[4]RIA, AstraZeneca, Pepparedsleden 1, 43183 Mölndal, Sweden

[5]CVMD, AstraZeneca, Pepparedsleden 1, 43183 Mölndal, Sweden

[6]Institució Catalana de Recerca i Estudis Avançats (ICREA), Passeig Lluís Companys 23, 08010 Barcelona, Spain

*Correspondence: anders.hogner@astrazeneca.com (A.C.H.), victor.guallar@bsc.es (V.G.), karl.edman@astrazeneca.com (K.E.)

http://dx.doi.org/10.1016/j.str.2015.09.012

SUMMARY

Steroid receptor drugs have been available for more than half a century, but details of the ligand binding mechanism have remained elusive. We solved X-ray structures of the glucocorticoid and mineralocorticoid receptors to identify a conserved plasticity at the helix 6–7 region that extends the ligand binding pocket toward the receptor surface. Since none of the endogenous ligands exploit this region, we hypothesized that it constitutes an integral part of the binding event. Extensive all-atom unbiased ligand exit and entrance simulations corroborate a ligand binding pathway that gives the observed structural plasticity a key functional role. Kinetic measurements reveal that the receptor residence time correlates with structural rearrangements observed in both structures and simulations. Ultimately, our findings reveal why nature has conserved the capacity to open up this region, and highlight how differences in the details of the ligand entry process result in differential evolutionary constraints across the steroid receptors.

INTRODUCTION

Biological functions originate from, and are maintained by, a combination of genomic drift and selection. The traditional method to derive evolutionary relationships is to compare primary sequences, tertiary structures, and protein function. However, while changes in the amino acid sequence and placement of key residues provide useful insights into lineage, this only provides the basic framework for mechanistic detail. A more complete functional understanding requires protein plasticity to be considered. Moreover, comparing protein flexibility of related systems adds an important dimension when exploring evolutionary trajectories (Bhabha et al., 2013).

The steroid receptor family consists of five closely related receptors: the mineralocorticoid receptor (MR), the glucocorticoid receptor (GR), the androgen receptor (AR), the progesterone receptor (PR), and the estrogen receptors (ERα and ERβ) (Figure 1A). All these receptors bind cholesterol derivatives and play a critical role in fundamental biological processes, ranging from pregnancy to early development, the stress response, and electrolyte homeostasis (Evans, 1988; Mangelsdorf et al., 1995). Continual pharmaceutical efforts have resulted in several efficacious drugs across the family (Cole, 2006; Gravez et al., 2013; Shelley et al., 2008; Sitruk-Ware and Nath, 2010; Alexander et al., 2013). However, target class-related side effects limit the prescription of these drugs for many indications, and the scope for further improvement is considered to be high (Bertocchio et al., 2011). The receptors share a common architecture with three separate domains: the N-terminal domain (NTD), the DNA binding domain, and the ligand binding domain (LBD). Besides recognizing the ligand pharmacophore, the LBD also contains the activation function 2 (AF-2), which is important for transmitting ligand binding information and partially driving the co-regulator interaction fingerprint (Gronemeyer et al., 2004). In the resting state, the receptors are associated with chaperone proteins in the cytoplasm. Ligand activation leads to a partial release of chaperone proteins, followed almost always by nuclear translocation. In the nucleus, the receptors dimerize and form ligand and context-specific protein complexes, resulting in activation and/or repression of gene transcription.

All steroid receptor LBD structures exhibit the typical three-layered α-helical fold that fully encloses the various compounds in the ligand binding pocket (Bledsoe et al., 2002; Williams and Sigler, 1998; Fagart et al., 2005; Matias et al., 2000) (Figure 1B). When overlaying the steroid receptors, the largest structural difference in proximity to the ligand is located in the region where helices 3, 7, and 11 meet (Li et al., 2005). Figure 1C shows a detailed comparison of GR with its paralog MR. An outward tilt of the helix 6–7 (H6-H7) interface in GR results in an expanded ligand binding pocket, and the most potent GR ligands contain large substituents extending in this direction

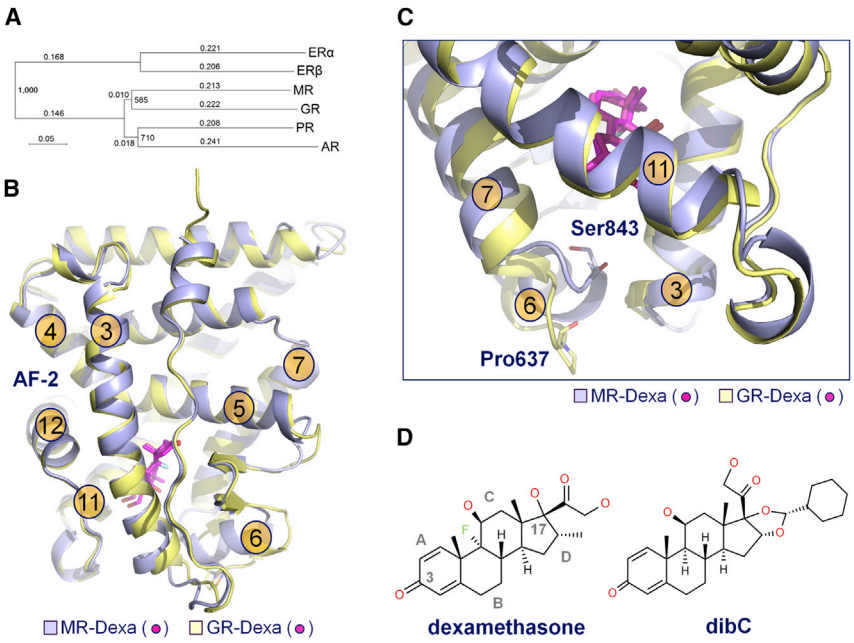

Figure 1. Evolutionary Relationship of the Steroid Receptors with Structural Comparison of GR- and MR-LBD

(A) Evolutionary relationship of the steroid hormone receptors (ERα, ERβ, MR, GR, PR, and AR). Decimal numbers = distance; integers = bootstrap value.

(B) GR (yellow) in complex with dexamethasone (magenta) overlaid on MR (light blue) in complex with dexamethasone (magenta). The AF-2 surface is located where helices 3, 4, and 12 meet.

(C) Details near the region where helices 3, 7, and 11 meet.

(D) The chemical structures of dexamethasone and dibC. The steroidal A, B, C, and D rings and positions 3 and 17 are marked on the dexamethasone structure.

(17α). Despite the smaller pocket in MR, several ligands with bulky 17α substituents on the steroidal D-ring, such as desisobutyrylciclesonide (dibC, the active metabolite of the prodrug ciclesonide), are more potent in the MR binding assay than the endogenous agonist aldosterone.

Plasticity in the H6-H7 region has been reported for ERα, AR, and PR (Andrieu et al., 2015; Nettles et al., 2007; Kohn et al., 2012), and appears to be a conserved feature across the nuclear receptor superfamily (Soisson et al., 2008; Hughes et al., 2012). To build a detailed understanding for how the differences in receptor design influence the H6-H7 rearrangements, we determined the X-ray structures of both MR and GR in complex with dexamethasone and dibC (Figure 1D). The structures revealed that when binding a ligand with a large 17α substituent, MR is fully capable of adopting an open structural conformation, and that the nature of these rearrangements is clearly distinct from analogous changes in GR. Why has nature preserved the capacity to open up this region across the steroid receptor family, even though it is not exploited by the endogenous ligands? Our hypothesis is that the observed plasticity is an integral part of the ligand entry mechanism.

To test this hypothesis, we performed comprehensive all-atom unbiased simulations. In these studies, we linked the observed plasticity in the H6-H7 region to the ligand binding mechanism. While the simulations clearly identified a common binding trajectory for the two receptors, they also highlighted detailed differences in the entry and exit processes. By employing surface plasmon resonance (SPR) and single-molecule microscopy (SMM), we showed that these differences correlate with distinct ligand-receptor residence times. Finally, we performed a bioinformatics analysis whereby we confirmed that GR has relaxed evolutionary constraints on the H6-H7 amino acid sequence relative all other steroid receptors. The link to the ligand binding utility provides a functional understanding for these observations.

RESULTS

A Conserved Plasticity

Dexamethasone was originally developed as a GR-specific agonist (Alexander et al., 2013) and was used to determine the first GR-LBD structure (Bledsoe et al., 2002). However, dexamethasone was later shown to also be a potent MR ligand in a functional reporter gene assay (Rupprecht et al., 1993). The X-ray structure of MR in complex with dexamethasone (MR:Dexa, Figure 2A) is similar to the corresponding GR:Dexa structure (normalized root-mean-square deviation [RMSD] of 0.37 Å for 100 C_α atoms) (Table 1). However, examining the region where helices 3, 7, and 11 meet confirms that the 17α subpocket is considerably smaller in the MR structure than in the GR structure (Figure 1C). This is reflected in the total volume of the MR:Dexa ligand binding pocket, which is approximately 543 $Å^3$ compared with 572 $Å^3$ in the GR:Dexa structure (Figure S1).

It has been proposed that structural differences in the loop between helices 6 and 7 are primarily due to replacement of $Ser843^{MR}$ by $Pro637^{GR}$, which alters the geometrical constraints of this region and allows GR to adopt a more open conformation (Li et al., 2005). However, despite the limited size of the MR subpocket, dibC has higher affinity than aldosterone in the scintillation proximity assay using tritiated aldosterone and MR-LBD fusion protein (K_i for dibC is 0.18 nM compared with 1.0 nM for aldosterone, Figure S2). To study the structural flexibility associated with large 17α substituents, we determined the complex structures of MR:dibC and GR:dibC (Table 1).

The structure of MR:dibC superimposes well on the MR:Dexa structure (normalized RMSD 0.28 Å for 100 C_α atoms). dibC is placed in a nearly identical position as dexamethasone in the binding pocket, with all polar interactions conserved (Figure 2B). In addition, the AF-2 surface remains virtually unchanged, with key interactions to the NCOA1 peptide intact. However, while these two receptor conformations are closely related, dibC induces a large rearrangement of the H6-H7 loop region, essentially extending the ligand binding pocket toward the receptor surface (Figure 3A). Specifically, side chains of $Ser843^{MR}$, $Met845^{MR}$, and $Cys849^{MR}$ in the MR:Dexa complex occupy the same volume as the cyclohexyl motif of dibC, forcing the

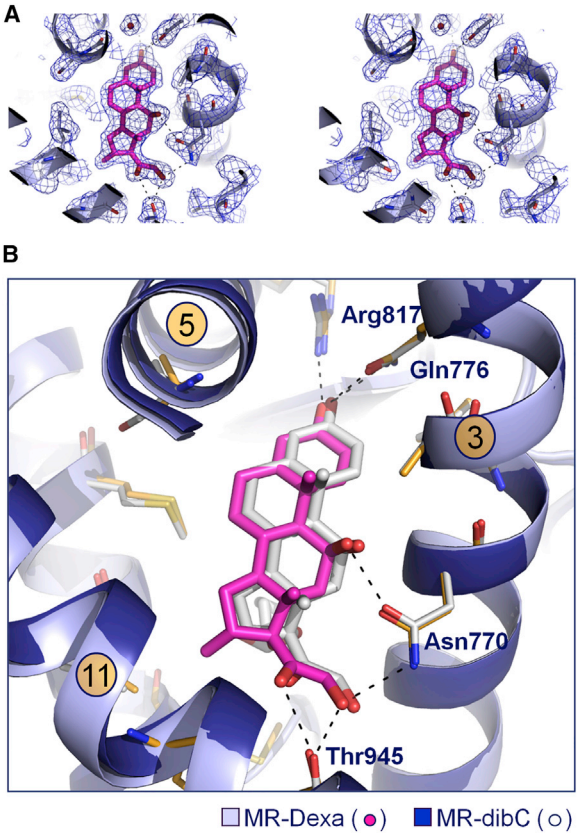

Figure 2. Comparison of the Complex Structures of MR:Dexa and MR:dibC

(A) Stereo view of the $2mF_o$-dF_c density map of the MR:Dexa ligand binding pocket.

(B) The structure of MR (light blue) in complex with dexamethasone (magenta) superimposed on MR (dark blue) in complex with dibC (white). The steroid template overlays nearly perfectly (RMSD 0.28 Å) with all hydrophilic interactions conserved.

receptor to adopt a new conformation (Figure 3B). This leads to a repositioning of helix 6 and an extension of helix 7. While $Ser843^{MR}$ was previously buried within the protein and engaged in a hydrogen bond to the backbone nitrogen of $Met845^{MR}$, it is now exposed to the solvent, forming the new start of helix 7 (Figure 3A). Recent data suggest that phosphorylation of this residue affects both ligand binding and receptor translocation into the nucleus (Shibata et al., 2013). The structural changes observed here explain how the receptor may use the local plasticity to make $Ser843^{MR}$ available for modification.

The size of the 17α pocket in the MR:dibC complex increases significantly (total ligand binding pocket volume 714 $Å^3$, Figure S1), and the superposition on the GR:Dexa structure shows that this region now adopts a more closely related structural state (Figure 3C). Finally, while GR in complex with dibC (Figure 3D) expands the 17α pocket (total ligand binding pocket volume 661 $Å^3$, Figure S1) relative to the GR:Dexa structure, it does not alter any of the secondary structural elements. Instead, the H6-H7 region appears to be shifted in a rigid way in response to cyclohexyl of dibC. While plasticity in the H6-H7 region seems to be conserved across these two receptors, the details of the ligand-driven rearrangements are different.

To quantify the flexibility in the H6-H7 region across the steroid receptor family, we performed principal component analysis for all X-ray structures from the PDB for each receptor. This allows visualization of the variance between structures as a set of normal modes. While the description of this variance will be highly dependent on what regions of the binding pocket are exploited by the various ligands, the mode describing H6-H7 motion is one of the strong features (Figure S3). However, for MR the H6-H7 motion is only prominent if we include the MR:dibC structure from this work, emphasizing that the MR:dibC structure describes a novel structural conformation.

Modeling Nonbiased Entry and Exit Pathways

Spontaneous ligand binding events have been investigated using molecular dynamics in both exposed (Buch et al., 2011) and partially exposed binding sites (Dror et al., 2011). However, nuclear receptors have fully occluded binding pockets that likely require significant rearrangements for ligand entry. Therefore, we decided to use protein energy landscape exploration (PELE) (Borrelli et al., 2005), an alternative approach that uses Monte Carlo algorithms with structural prediction for efficient sampling of the protein-ligand energy landscape. For ligand escape simulations, the MR and GR X-ray complex structures were used as the starting position. For ligand binding studies, the ligand was randomly placed in the bulk solvent and allowed to freely migrate. All simulations were completed in the presence and absence of a co-factor peptide at the AF-2 site (NCOA1 residues 1,430–1,441 for MR and NCOA2 residues 741–753 for GR). In addition, both the wild-type protein sequences and the specific mutants present in the X-ray structures were used.

Ligand Dissociation

For all permutations of both MR and GR, we performed three separate exit simulations, observing only one exit trajectory perforating the surface where helices 3, 7, and 11 meet. Figure 4A illustrates the MR:Dexa exit pathway simulation with the array of dexamethasone positions superimposed on the initial MR structure. Notably, ligand motion is coupled with significant rearrangement of the protein backbone along the migration pathway. In particular, the loop connecting helices 6 and 7 is shifted outward to accommodate ligand release (Figure 4B). Interestingly, the simulated protein movements mimic the differences between the MR:Dexa and MR:dibC structures shown in light and dark blue, respectively. Root-mean-square fluctuations (RMSF) along the exit trajectory (Figure 4C) clearly show that the movements of the H6-H7 region are considerably larger than for the rest of the protein.

Figure 5 shows the corresponding simulation for GR:Dexa (equivalent simulations for MR:dibC and GR:dibC resulted in the same exit trajectory). Based on the complete set of ligand dissociation simulations it is apparent that both MR and GR have the same ligand unbinding pathway. In addition, while ligand exit is associated with similar protein motions, the fluctuations in the H6-H7 region are significantly larger for MR than for GR (Figure 5C). This is in agreement with the idea that GR would require smaller rearrangements, because the receptor is more open to begin with.

Table 1. Data Collection and Refinement Statistics

	MR:Dexa	MR:dibC	GR:Dexa	GR:dibC
Data Collection[a]				
PDB ID	4UDA	4UDB	4UDC	4UDD
Space group	P212121	P41212	P3221	P3221
a, *b*, *c* (Å)	73.00, 81.40, 45.23	75.92, 75.92, 117.00	84.66, 84.66, 105.91	87.20, 87.20, 102.89
α, β, γ (°)	90.00, 90.00, 90.00	90.00, 90.00, 90.00	90.00, 90.00, 120.00	90.00, 90.00, 120.00
Resolution (Å)	40.7–2.03 (2.17–2.03)	48.79–2.36 (2.55–2.36)	31.81–2.50 (2.67–2.50)	40.14–1.80 (1.85–1.80)
R_{sym} (R_{merge})	0.06 (0.50)	0.13 (1.30)	0.08 (0.55)	0.08 (1.05)
$I/\sigma I$	13.10 (2.30)	15.10 (1.90)	8.80 (1.60)	7.40 (0.70)
Completeness (%)	83.9 (83.7)	100.0 (100.0)	99.6 (99.5)	99.9 (100.0)
Redundancy	3.3 (2.5)	12.6 (11.7)	4.1 (4.2)	3.5 (3.6)
Refinement				
Resolution (Å)	2.03	2.36	2.50	1.80
No. of reflections	15,085	14,672	15,559	42,339
R_{work}/R_{free}	0.185/0.240	0.182/0.218	0.210/0.253	0.213/0.224
No. of atoms				
Protein	2,080	2,118	2,133	2,184
Ligand/ion	34	49	64	146
Water	101	60	83	250
B factors				
Protein	30.14	53.25	49.72	33.25
Ligand/ion	22.12	44.16	34.51	23.55
Water	36.03	56.86	46.23	46.95
RMSD				
Bond lengths (Å)	0.010	0.010	0.010	0.010
Bond angles (°)	1.01	1.04	1.12	1.06
MolProbity score				
Clashscore	2	1	1	1
Ramachandran outliers (%)	0	0	0.4	0
Side-chain outliers (%)	1.7	1.7	2.5	0.8

[a]Values in parentheses represent highest-resolution shell.

Ligand Association

To investigate ligand entry, we randomly placed dexamethasone in the bulk solvent and released it to freely probe the protein surface. For each receptor we performed five runs with 64 independent trajectories over 48 hr. Each run yielded one to two trajectories whereby the ligand entered the binding pocket. In all runs the ligand is free to move without any predefined search direction.

Figure 6A shows the evolution of the ligand heavy atom RMSD to the crystallographic complex for one of the MR:Dexa runs. It is clear that most of the trajectories explore the receptor surface with some excursions into the bulk solvent. However, the blue and red trajectories enter the ligand binding pocket at steps ~50 and ~210, respectively. While the entry along the blue trajectory is relatively fast, the red demonstrates the unbiased nature of the simulation, probing a large portion of the receptor surface before finding the entrance pathway. Figure 6B shows representative ligand centers of mass along these trajectories superimposed on the initial protein structure, with the entry to the binding pocket denoted by a surface representation. The corresponding ligand entry simulation for GR is shown in Figure S4. In keeping with the ligand escape simulations for all runs in both systems, trajectories entering the ligand binding pocket pierce the protein surface at the H3-H7-H11 junction. The MR:Dexa binding event is demonstrated in greater detail in the Movie S1.

While the mutants used in the X-ray structures did not influence the simulations significantly, removal of co-factor peptide at the AF-2 resulted in larger fluctuations in both helix 12 and the H3-H7-H11 junction along the exit and entrance trajectories. However, the ligand entry pathway remained unchanged. The presence of co-regulator peptide has been shown to affect the ligand binding kinetics (Pfaff and Fletterick, 2010).

Active-Site Ligand Refinement and Binding Free Energy

Once the entrance path to the MR binding pocket had been located, we refined the free search with local enhanced sampling to obtain a precise pose for the best binder. This procedure does not add any bias in the ligand search direction, but limits the sampling to the region around the entrance point (typically 10–15 Å). Figure 7A shows the interaction energy profile plotted against the ligand heavy atom RMSD to the crystallographic complex for the MR:Dexa refining process (400 trajectories).

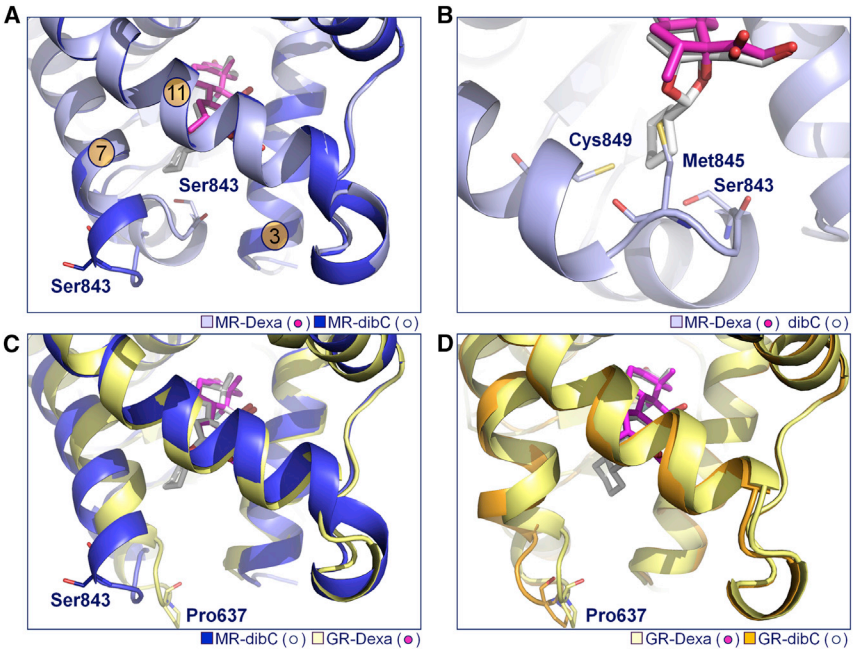

Figure 3. Comparison of the Complex Structures of MR:Dexa, MR:dibC, GR:Dexa, and GR:dibC

(A) MR (light blue) in complex with dexamethasone (magenta) overlaid on MR (dark blue) in complex with dibC (white).

(B) The cyclohexyl motif of dibC comes into direct conflict with residues from H7 (MR:Dexa), enforcing a new structural state.

(C) MR (dark blue) in complex with dibC (white) superimposed on GR (yellow) in complex with dexamethasone (magenta).

(D) GR (yellow) in complex with dexamethasone (magenta) overlaid on GR (orange) in complex with dibC (white).

The lowest binding energies are derived from poses located within 0.75 Å RMSD of the X-ray ligand conformation. The sampling places dexamethasone in the accurate orientation with the A-ring 3-keto moiety pointing toward the $Arg817^{MR}$-$Gln776^{MR}$ pair from helices 5 and 3, and the D-ring hydroxyacetyl approaching the $Asn770^{MR}$ on the N-terminal half of helix 3 (Figure 7B). Studying the protein-ligand interaction energy plot in more detail (Figure 7A), it is interesting that the surface exploration exhibits local minima near RMSD of 12 Å. In the crystal structure of GR:Dexa and GR:dibC, this site is occupied by a steroid-like CHAPS molecule that is part of the protein formulation (Figure S5). In addition, for MR a nonsteroidal antagonist has been observed at this position (Hasui et al., 2011). As such, the region may correspond to a peripheral binding site at the H3-H7-H11 junction, and the energy barrier located at the 11- to 12-Å segment in Figure 7A reflects the energy cost associated with the surface-crossing event through the entry channel.

The fast performance of PELE, together with the local restriction in the refinement exploration, facilitates running hundreds of trajectories. Based upon Markov state model (MSM) analysis (Takahashi et al., 2014), we used these data to calculate the binding free energies for MR:Dexa and MR:dibC. While absolute values might be slightly shifted due to the absence of an exhaustive surface/bulk exploration, relative values should be in reasonable agreement, because both ligands share entry point and binding site. Figure 7C shows a 2D projection of the potential mean field (PMF) obtained for MR:Dexa along the 400 refinement trajectories. The red area corresponds to the bulk exploration, whereas the global minimum, shown in blue, corresponds to ligand positions matching the experimental structure (Figures 7A and 7B). Integration of the PMF volume at the active site,

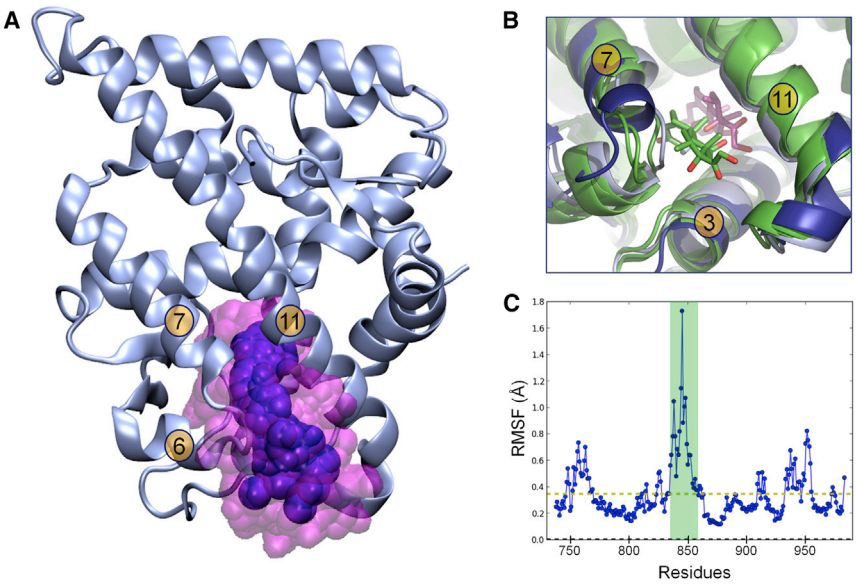

Figure 4. Ligand Exit Pathway for the MR:Dexa Complex

(A) The ligand center of mass is highlighted as blue beads. The ligand atoms are shown as transparent space fill.

(B) Detail of the backbone rearrangement along the exit pathway. The MR:Dexa and MR:dibC X-ray structures are shown in light and dark blue, respectively, with dexamethasone in the binding pocket in magenta. Three protein cartoon snapshots and one pose of dexamethasone as it passes through the receptor surface from the exit simulations are shown in green.

(C) C_α RMSF relative the average structure along the MR:Dexa exit pathway plotted for each residue. The dotted line denotes the average RMSF across the LBD. Helices 6 and 7 are marked with green shading.

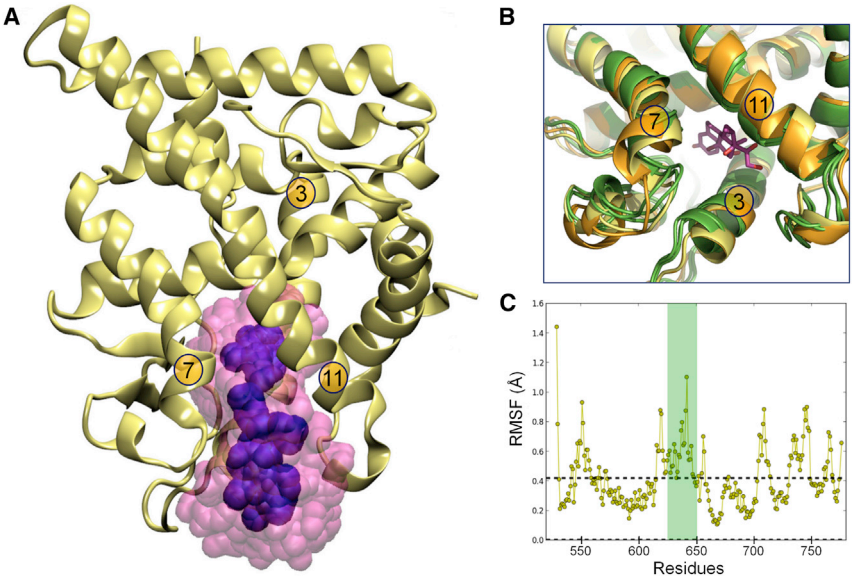

Figure 5. Ligand Exit Pathway for the GR:Dexa Complex

(A) The ligand center of mass is highlighted as blue beads. The ligand atoms are shown as transparent space fill.

(B) Detail of the backbone rearrangement along the exit pathway. The GR:Dexa and GR:dibC X-ray structures are shown in light yellow and orange, respectively. Three snapshots from the exit simulations are shown in green, and dexamethasone in the binding pocket is shown for reference in magenta.

(C) C_α RMSF relative the average structure along the GR:Dexa exit pathway where helices 6 and 7 are marked with green shading.

where we observe a smooth function (as opposed to the bulk solvent or entrance pathway), converges to a binding free energy of −7.5 kcal/mol for dexamethasone and −9.3 kcal/mol for dibC. The difference in binding free energy of 1.8 kcal/mol is in quantitative agreement with the experimental difference of 2.09 kcal/mol (derived from the K_i values of 6.3 nM for dexamethasone and 0.18 nM for dibC).

Residence Time Measurements

The ligand entry and exit mechanism establishes a functional role for helices 6 and 7 as a gatekeeper. In addition, the simulations revealed that the structural rearrangements required for ligand entry and exit are significantly different for GR and MR. As a consequence, the ligand binding kinetics should differ for the two receptors. Using both SPR and SMM (Gunnarsson et al., 2015), we measured the residence time of both dexamethasone and dibC by monitoring the time-resolved change in receptor binding to a surface-immobilized co-regulator peptide upon addition of >10-fold concentration excess of a reference compound (Figure S6). The data from all experiments are summarized in Table 2. In all instances, k_{off} is larger for GR than for MR, hence the residence time is longer in MR. This is in agreement with the observations that MR requires a larger rearrangement of the H6-H7 region compared with GR (Figures 4 and 5). In addition, dexamethasone has a larger k_{off} than dibC, reflecting the fact that dibC is a bulkier ligand. Finally, while the different measurement methods result in the same pattern for both GR and MR and dexamethasone and dibC, providing confidence to the analysis, the systematically larger off rates using SMM likely reflect the temperature difference at which the experiments were conducted (20°C for SMM and 10°C for SPR).

Differential Selection Pressure

Studies on the evolution of GR from the ancestral corticoid receptor revealed that GR has accumulated a number of mutations on and in the proximity of helix 7 that prevents reversal of evolution (Bridgham et al., 2009). As our findings suggest that there is an intimate link to the ligand binding function, we decided to investigate the evolutionary consequences across the whole steroid receptor family. To explore this, sequence clusters for each receptor were downloaded from OrthoDB (Waterhouse et al., 2013). The sequences for each receptor were aligned using ClustalX version 2.0 (Larkin et al., 2007) and the pairwise species overlap with GR was selected for each receptor. Each residue position was then assigned a variability score based on the number of different amino acids at that position across the various species. All receptor sequences were overlaid on the GR

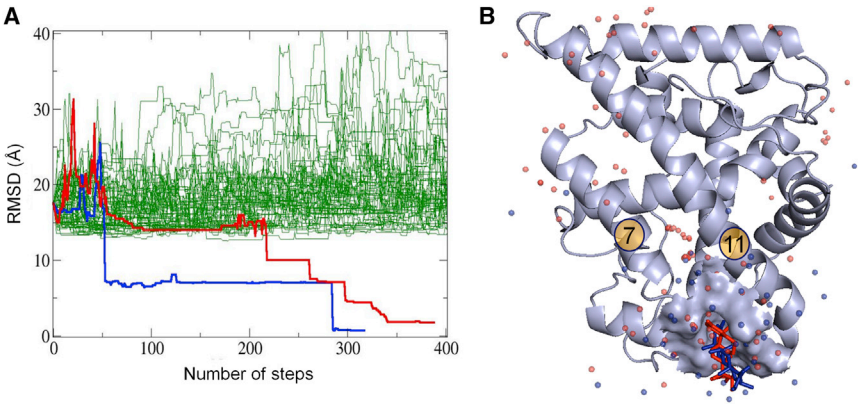

Figure 6. Unbiased Simulation of Dexamethasone Entering the MR Binding Pocket

(A) Each line represents the ligand heavy atom RMSD to the ligand from the crystallographic structure for a single trajectory. Two of the trajectories represented by blue and red lines enter the ligand binding pocket at steps 52 and 214, respectively.

(B) The ligand center of mass for the two trajectories that enter the binding pocket are shown as blue and red spheres. The region where the ligands enter the binding pocket is emphasized as a surface with two ligands from the simulations shown in full stick representation.

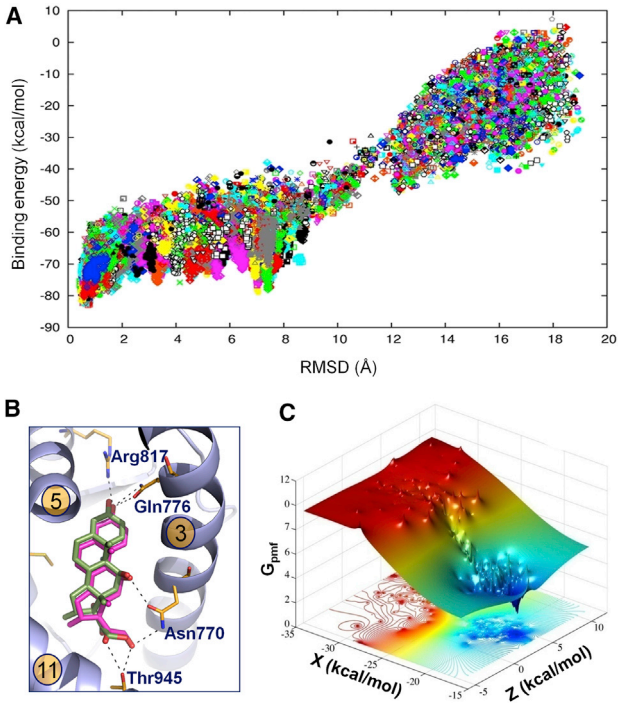

Figure 7. Refined Ligand Binding Simulations and Estimated Binding Free Energy

(A) The protein-ligand interaction energy plotted against the ligand heavy atom RMSD to the crystallographic structure along the 400 refinement trajectories in MR:Dexa.

(B) MR (blue) in complex with dexamethasone (magenta) overlaid on the lowest interaction energy structure after the refined exploration (green).

(C) X-Z 2D projection of the PMF obtained in the MSM analysis for the same process.

sequence using X-ray structures to define the equivalent positions. Finally, we plotted the variability score against the amino acid sequence for all receptor pairs (Figure 8). The data confirm that important structural elements of the receptors are relatively conserved. For example, the variability score for the AF-2 surface (the N-terminal end of H12, H4, and the C-terminal end of H3), which is directly involved in the protein-protein interaction transmitting the ligand activation signal, is consistently low for all receptors. However, H6-H7 exhibits a greater variability score in GR relative to all other receptors. Interestingly, GR also has a segment of higher variability near the C-terminal end of H11. This region sits directly across from the N-terminal end of H7 (Figure 1C), and it is conceivable that amino acid sequences of these regions may well co-vary with each other. Figure S7A shows the variability score for the individual amino acids in the H6-H7 region for the full set of GR species. It is clear that the high variability score of the region resides in discrete positions (primarily in residues 631, 632, 635, 638, and 640). These residues are all located on the outside of the receptor in both the GR:Dexa and GR:dibC structures (Figure S7B).

DISCUSSION

The fundamental role and mechanism of action of steroid receptors have been studied extensively, yet details of the ligand binding mechanisms have remained unclear. By comparing the structures of MR and GR in complex with dexamethasone and dibC, we confirmed the intrinsic capacity to open up the H6-H7 region. While the GR:Dexa structure adopts an open conformation compared with the MR:Dexa complex, the MR:dibC structure is able to extend the ligand binding pocket significantly and adopt a structural state akin to the GR:Dexa arrangement. Studies of ancestral corticoid receptor (AncCR), the common predecessor of MR and GR, revealed that the $Ser106^{AncCR}$ (corresponding to $Ser843^{MR}$) to $Pro637^{GR}$ switch was a permissive mutation that facilitated a subsequent $Leu111^{AncCR}$ (corresponding to $Leu848^{MR}$) to $Gln642^{GR}$ mutation (Bridgham et al., 2006). This is an example of conformational epistasis and has played an important role in the evolution of GR hormone selectivity (Ortlund et al., 2007). We show that GR and MR demonstrate a similar capacity to form an open conformation, and it is likely that the AncCR also exhibited the same flexibility. Hence, as GR evolved from AncCR, the $Ser106^{AncCR}$ to $Pro637^{GR}$ mutation would primarily serve to select a subset of preexisting structural states, rather than creating a completely new arrangement. The importance of conformational selection over induced fit has provided mechanistic insights for several biological systems (Changeux, 2013), and it is plausible that evolution through mutation often operates in an analogous way.

Table 2. Measurement of k_{off} Using SPR and SMM

Ligand (Method)	GR (s^{-1})	MR (s^{-1})
Dexa (SPR, 10°C)	0.0034	0.0011
dibC (SPR, 10°C)	0.0010	<0.0001
Dexa (SMM, 20°C)	0.0070	0.0025
dibC (SMM, 20°C)	0.0029	0.0012

Extensive ligand binding simulations revealed that the entry and exit trajectories all pass through the H3-H7-H11 junction. As the ligands cross the receptor surface, the outward bending motion of the H6-H7 region is qualitatively similar to the observed perturbations caused by the large 17α cyclohexyl substituent in the dibC complex structures, linking the observed H6-H7 plasticity to the ligand binding mechanism. Interestingly, H7 has also been shown to be important for dimerization of several nuclear receptors (Osz et al., 2012). This suggests that the two functions could be linked for these receptors, but the strength of this relationship remains to be determined. The results from the ligand binding simulations indicate that large-amplitude protein motions of helix 12, as suggested by apo and holo crystallographic nuclear hormone receptors (Moras and Gronemeyer, 1998; Yen, 2001; Brzozowski et al., 1997), are not required for ligand entry. Instead, the conformation of the LBD is likely to resemble the ligand bound agonistic conformations of the receptors during the ligand entry step (Capelli et al., 2013; Batista and Martínez, 2013). We show that small-scale vibrations combined with a structural rearrangement of H6-H7 region are enough to identify an energetically favorable pathway to allow the ligands to diffuse into the binding pocket. In contrast to other modeling studies using biased protocols, we do not observe multiple ligand entry or exit pathways (Capelli et al., 2013; Sonoda et al., 2008; Aci-Sèche et al., 2011). Finally, careful analysis of the binding energies along the entry trajectory revealed a

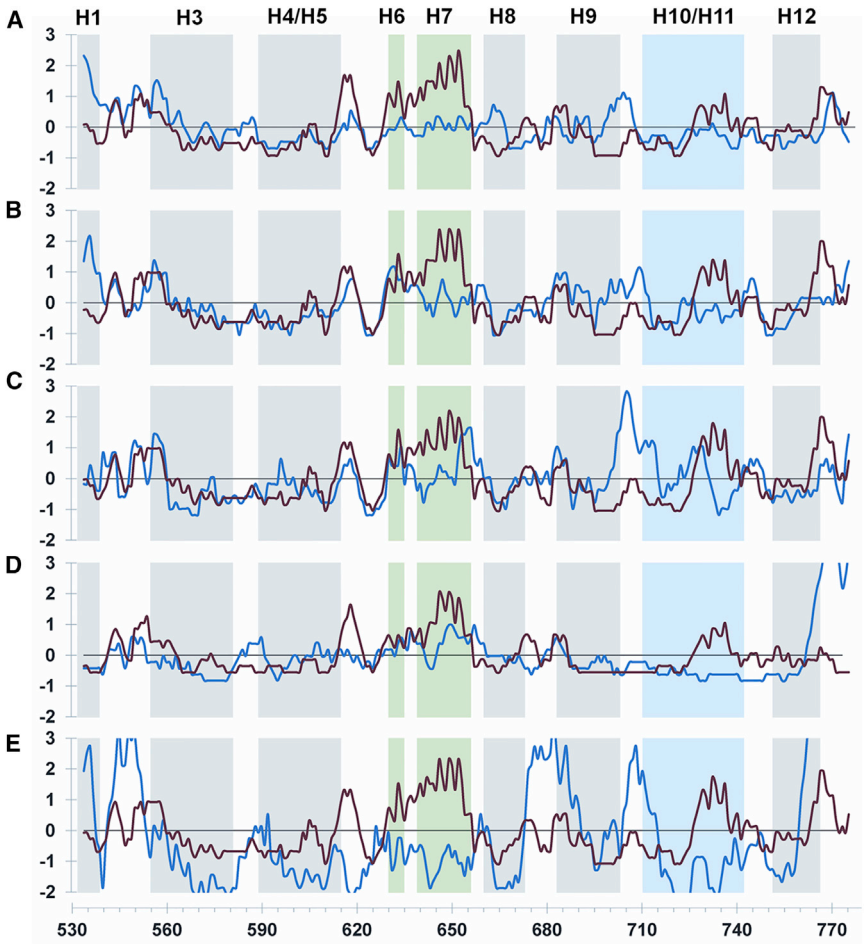

Figure 8. Evolutionary Conservation of the LBD for the Steroid Receptors

The graphs show normalized amino acid variability score for pairwise comparisons of MR (A), PR (B), AR (C), ERα (D), and ERβ (E) in blue versus GR in red plotted against the GR amino acid sequence. The variability score was average normalized and smoothed using a five-amino-acid sliding window. Helices 1–12 are annotated using vertical bars (green: H6–7; blue: H10–11; gray: all others). High variability scores indicate less conservation.

potential peripheral binding site. While it requires further characterization, the function of such a site on the surface of the receptor could serve to capture the ligands and increase the chances for productive binding events.

It is firmly established that steroid receptors depend on a number of chaperone and co-chaperone proteins for correct folding that is capable of high-affinity hormone binding (Grad and Picard, 2007). Although the ligand entry function is likely to have evolved before the synergies with chaperone proteins, these proteins will nevertheless limit the access to the receptors and thereby form boundary conditions for any ligand entry hypothesis. Mutation and peptide competition studies suggest that Hsp90 interacts at the AF-2 surface (Ricketson et al., 2007; Fang et al., 2006). In addition, co-chaperones have been mapped to interact with regions surrounding the C-terminal end of H1 and the N-terminal end of H3 (Caamaño et al., 1998), and with the loop that connects them (Cluning et al., 2013). Neither of these areas overlap with the entry site proposed here. However, previous studies have shown that the chaperone complex promotes the ligand binding process (Grad and Picard, 2007). Interestingly, the simulations whereby we removed the co-regulator peptides resulted in greater fluctuations in both the H3-H7-H11 junction and H12. These results suggest that the presence of chaperone proteins at remote sites can allosterically influence the ligand entry process proposed here.

While the dibC complex structures show that both corticoid receptors can adopt an open conformation, they also highlight that the plasticity in the H6-H7 region is different. For MR, the challenge from a large 17α substituent results in a complete rearrangement of the H6-H7 structure. In contrast, GR responds with a rigid shift of the region. A closer inspection of the simulations revealed ensuing differences as MR require larger rearrangements in the gatekeeper residues for productive ligand binding and unbinding. This is in agreement with the kinetic measurements revealing that both dexamethasone and dibC exhibit longer receptor residence times in MR than in GR. However, these observations do not necessarily result in differences in ligand affinity per se, as both ligand entry and exit will be governed by the same plasticity, potentially affecting on and off rates equally. Nevertheless, it is important to note that ligand binding and unbinding are asymmetric events. While ligand binding occurs with the receptor in the chaperone complex in the cytoplasm, unbinding will likely occur in the different protein complex. As such, it is tempting to speculate that the relative stabilization of the open versus the closed conformation may differ for the two states. This could increase the apparent ligand affinity and potentially add another layer of differentiation. To resolve this, detailed structural information on the relevant protein complexes would be required.

The distinct receptor blueprints also appear to have evolutionary consequences. By comparing the amino acid sequence for different species across all steroid receptors, we found that GR exhibits a higher mutational frequency in the H6-H7 region. We propose that as GR evolved a cortisol selectivity profile, the change in the dynamic profile of the H6-H7 region, through the $Ser106^{AncCR}$ to $Pro637^{GR}$ mutation, altered the boundary conditions for the ligand entry mechanism. While for MR, residues need to be compatible with two distinct structural states during ligand entry, for GR the equivalent residues will be exposed to the solvent throughout the process. As a result the selection pressure was relaxed for specific positions in this region for GR, which explains why subsequent mutations could build.

The tremendous growth in the number of available X-ray structures from increasingly more advanced protein classes and complexes provides a plethora of snapshots of molecular mechanisms in action. However, to bridge the gap to detailed mechanistic insights and to establish evolutionary relationships, orthogonal data from biochemical experiments and in silico modeling are required. By combining information from several X-ray structures, extensive simulations, kinetic measurements, and bioinformatics analyses, we have uncovered the ligand binding mechanism into the occluded binding pocket of steroid hormone receptors. Ligand binding to the steroid receptors marks the first step in a chain of events that in the end triggers both broad genomic and nongenomic mechanisms. Understanding the details of ligand association and dissociation may facilitate the rational design of molecules that exploit the plasticity of the entry and exit processes to a greater extent. This could yield ligands with different modes of action, such as antagonists that block nuclear translocation or agonists with extended receptor occupancy and a prolonged pharmacological response.

EXPERIMENTAL PROCEDURES

Protein Expression, Purification, Crystallization, Structure Determination, and Analyses

The detailed protocols are described in the Supplemental Experimental Procedures. For structure, the following protein constructs were used: GR:Dexa, GR-LBD (amino acids 500–777) N517D, F602S, C638D; GR:dibC, GR-LBD (amino acids 500–777) N517D, V571M F602S, C638D; MR:Dexa, MR-LBD (amino acids 735–984) C808S, C910S; MR:dibC, MR-LBD (amino acids 735–984) C808S, S810L, C910S. For the kinetic measurements, the following constructs were used: GR, GR-LBD (NR3C1; amino acids 529–777); MR, MR-LBD (amino acids 712–984) C808S.

Mineralocorticoid Receptor Ligand Competition Binding Assay

A scintillation proximity-based radioligand binding assay was used to measure the ligand displacement of aldosterone to human MR-LDB. The detailed protocol is presented in the Supplemental Experimental Procedures.

PELE Simulations

Systems Setup

Initial coordinates for GR and MR were obtained from the crystals presented here. Three different receptor models were prepared: (1) the crystallographic structures, (2) the wild-type receptors generated by reverting the crystallographic mutations with the Schrödinger package (Schrödinger, 2013), and (3) the wild-type receptors in absence of the peptide co-factor. All structures were preprocessed with the protein preparation wizard (Madhavi Sastry et al., 2013) available in the Schrödinger package, adding hydrogen atoms and optimizing the hydrogen bond network, followed by a final visual inspection.

PELE Sampling

PELE combines a Monte Carlo approach with protein structure prediction methods, allowing exploration of long-timescale atomic biophysical processes (Borrelli et al., 2005; Cossins et al., 2012). Three main steps define the algorithm: (1) protein backbone and ligand perturbation, (2) specific side-chain sampling, and (3) global minimization (for more details see, for example, Kotev et al., 2015). The program uses an OPLS (Optimized Potentials for Liquid Simulations) all-atom force field with an implicit SGB (surface-generalized Born) continuum solvent model.

Ligand Exit Simulations

From the crystallographically prepared models, the exit protocol included random ligand's translations of 0.8 Å and rotation of 0.2 radians. The backbone perturbation included the lowest six anisotropic network model modes with maximum displacements of each α carbon up to 1 Å. A spawning criteria of 4 Å was used: any ligand whose center of mass is 4 Å behind the structure with the center of mass farthest coordinates (with respect to the initial position), in any direction, will abandon its position and continue the execution with the coordinates from the leading (farthest) one. Thus, all processors search collectively, with no bias in direction, for an effective escape path. Simulations were finished after the ligand's solvent-accessible area was larger than 0.5, with typical simulations times of 10–20 CPU hr.

Ligand Entrance Simulations

Starting from 20 conformations where the ligand is randomly distributed over the protein surface, free search simulations were performed with runs of 64 independent simulations (no spawning criteria were used) for 48 CPU hr. Ligand perturbation included equally probable translations of 3.0 Å/1.0 Å and rotation of 0.25/0.05 radians. Ligand displacement direction was randomly updated every six steps, thus ensuring that trajectories explored the entire surface. Furthermore, keeping the perturbation direction for six steps is necessary to observe entrance events in difficult cases.

Residence Time Determination

Residence time measurements of GR/MR:dexamethasone and dibC were determined using SMM and SPR (Biacore). In brief, GR/MR was preequilibrated with dexamethasone/dibC. Directly after addition of budesonide/aldosterone, the rate of receptor binding to the surface-immobilized co-factor peptide, caused by the ligand-induced change in affinity, was monitored continuously over ~15 min with SMM or by consecutive injection cycles (typically six) in SPR. See the Supplemental Information for details on surface preparation and experimental procedures. The dissociation rate was determined by exponential fits to the change in binding rate as a function of time.

Sequence Homology Analysis

Sequence clusters for each receptor were downloaded from the OrthoDB database (Waterhouse et al., 2013) by searching for the human ENS gene ID and selecting the vertebrate subset. For each receptor, sequences with a length two SDs below average length or that contained more than 100 "X" (unknown amino acids) were removed. The sequences for each receptor were aligned using ClustalX version 2.0 (Larkin et al., 2007), then further filtered to only keep sequences with an intact H6-H7 region (maximum 1 indel or "X" and $\geq$50% identity to the human H6-H7 region; sequences with large indels in H6-H7 were removed followed by realignment and refiltering to correct for alignment errors around indels). The filtered sets were scored using custom perl scripts; for each position in the alignment, a variability score was calculated by counting the number of different types of amino acids (i.e. if a position contained 5F, 3Y, and 9L, then the score is 3). To remove bias stemming from the inclusion of sequences from different species across the various receptors, we generated subsets wherein the same species were included for pairs of GR with either of (MR, PR, AR, ERα, ERβ). The paired subsets were realigned for each receptor, and the resulting alignments were analyzed and scored as previously described. Finally, the scores were normalized (variability score minus average variability score for LBD) and smoothed using a sliding window of five amino acids, and plotted against the GR protein sequence.

Phylogenetic Analysis of the Human LBD Region

Human sequences for the studied nuclear receptors (AR, ERα, ERβ, GR, MR, and PR) were extracted from the aforementioned dataset. Sequences were trimmed so that only the LBD region remained, aligned using ClustalX, and manually edited based on the structure (minor adjustments). The tree was calculated using ClustalX (bootstrap 1,000 iterations) and visualized using NJplot version 2.3 (Perrière and Gouy, 1996).

SUPPLEMENTAL INFORMATION

Supplemental Information includes Supplemental Experimental Procedures, seven figures and one movie and can be found with this article online at http://dx.doi.org/10.1016/j.str.2015.09.012.

AUTHOR CONTRIBUTIONS

K.E., A.C.H., M.L., and V.G. designed the research. U.K. performed binding experiments. S.B., C.K., T.J.J., A.C., and E.N. expressed and purified protein.

A.A. and L.W. crystallized the proteins. K.E. performed the structural determination and analyzed the data. C.G. performed the principal component analysis. A.H. performed the exit and entry simulations. D.L. and R.T. performed MSM analysis. A.G.,T.K., and S.G. performed the kinetic experiments. M.K.B. carried out the bioinformatics analysis.

ACKNOWLEDGMENTS

This study was supported by European Research Council 2014-PoC-eDrug to V.G. and by the SEV-2011-00067 grant of the Severo Ochoa Program. We would like to acknowledge our AstraZeneca colleagues J. Hartleib, R. Unwin, and R. Knöll for helpful discussions. We also thank N. Blomberg (ELIXIR) and R. Neutze (University of Gothenburg) for careful reading of the manuscript.

Received: June 25, 2015
Revised: September 3, 2015
Accepted: September 4, 2015
Published: October 22, 2015

REFERENCES

Aci-Sèche, S., Genest, M., and Garnier, N. (2011). Ligand entry pathways in the ligand binding domain of PPARγ receptor. FEBS Lett. *585*, 2599–2603.

Alexander, S.P.H., Benson, H.E., Faccenda, E., Pawson, A.J., Sharman, J.L., Spedding, M., Peters, J.A., and Harmar, A.J.; CGTP Collaborators (2013). The concise guide to pharmacology 2013/14: nuclear hormone receptors. Br. J. Pharmacol. *170*, 1652–1675.

Andrieu, T., Mani, O., Goepfert, C., Bertolini, R., Guettinger, A., Setoud, R., Uh, K.Y., Baker, M.E., Frey, F.J., and Frey, B.M. (2015). Detection and functional portrayal of a novel class of dihydrotestosterone derived selective progesterone receptor modulators (SPRM). J. Steroid Biochem. Mol. Biol. *147*, 111–123.

Batista, M.R., and Martínez, L. (2013). Dynamics of nuclear receptor helix-12 switch of transcription activation by modeling time-resolved fluorescence anisotropy decays. Biophys. J. *105*, 1670–1680.

Bertocchio, J., Warnock, D.G., and Jaisser, F. (2011). Mineralocorticoid receptor activation and blockade: an emerging paradigm in chronic kidney disease. Kidney Int. *10*, 1051–1060.

Bhabha, G., Ekiert, D.C., Jennewein, M., Zmasek, C.M., Tuttle, L.M., Kroon, G., Dyson, H.J., Godzik, A., Wilson, I.A., and Wright, P.E. (2013). Divergent evolution of protein conformational dynamics in dihydrofolate reductase. Nat. Struct. Mol. Biol. *11*, 1243–1249.

Bledsoe, R.K., Montana, V.G., Stanley, T.B., Delves, C.J., Apolito, C.J., McKee, D.D., Consler, T.G., Parks, D.J., Stewart, E.L., Willson, T.M., et al. (2002). Crystal structure of the glucocorticoid receptor ligand binding domain reveals a novel mode of receptor dimerization and coactivator recognition. Cell *110*, 93–105.

Borrelli, K.W., Vitalis, A., Alcantara, R., and Guallar, V. (2005). Protein energy landscape exploration. A novel Monte Carlo technique. J. Chem. Theor. Comput. *6*, 1304–1311.

Bridgham, J.T., Carroll, S.M., and Thornton, J.W. (2006). Evolution of hormone-receptor complexity by molecular exploitation. Science *312*, 97–101.

Bridgham, J.T., Ortlund, E.A., and Thornton, J.W. (2009). An epistatic ratchet constrains the direction of glucocorticoid receptor evolution. Nature *461*, 515–520.

Brzozowski, A.M., Pike, A.C., Dauter, Z., Hubbard, R.E., Bonn, T., Engström, O., Ohman, L., Greene, G.L., Gustafsson, J.A., and Carlquist, M. (1997). Molecular basis of agonism and antagonism in the oestrogen receptor. Nature *389*, 753–758.

Buch, I., Giorgino, T., and De Fabritiis, G. (2011). Complete reconstruction of an enzyme-inhibitor binding process by molecular dynamics simulations. Proc. Natl. Acad. Sci. USA *108*, 10184–10189.

Caamaño, C.A., Morano, M.I., Dalman, F.C., Pratt, W.B., and Akil, H. (1998). A conserved proline in the hsp90 binding region of the glucocorticoid receptor is required for hsp90 heterocomplex stabilization and receptor signaling. J. Biol. Chem. *273*, 20473–20480.

Capelli, A.M., Bruno, A., Guadix, A.E., and Costantino, G. (2013). Unbinding pathways from the glucocorticoid receptor shed light on the reduced sensitivity of glucocorticoid ligands to a naturally occurring, clinically relevant mutant receptor. J. Med. Chem. *56*, 7003–7014.

Changeux, J.P. (2013). 50 years of allosteric interactions: the twists and turns of the models. Nat. Rev. Mol. Cell Biol. *14*, 819–829.

Cluning, C., Ward, B.K., Rea, S.L., Arulpragasam, A., Fuller, P.J., and Ratajczak, T. (2013). The helix 1-3 loop in the glucocorticoid receptor LBD is a regulatory element for FKBP cochaperones. Mol. Endocrinol. *27*, 1020–1035.

Cole, T.J. (2006). Glucocorticoid action and the development of selective glucocorticoid receptor ligands. Biotechnol. Annu. Rev. *12*, 269–300.

Cossins, P.B., Hosseini, A., and Guallar, V. (2012). Exploration of protein conformational change with PELE and meta-dynamics. J. Chem. Theor. Comput. *8*, 959–965.

Dror, R.O., Pan, A.C., Arlow, D.H., Borhani, D.W., Maragakis, P., Shan, Y.B., Xu, H.F., and Shaw, D.E. (2011). Pathway and mechanism of drug binding to G-protein-coupled receptors. Proc. Natl. Acad. Sci. USA *108*, 13118–13123.

Evans, R.M. (1988). The steroid and thyroid hormone receptor superfamily. Science *240*, 889–895.

Fagart, J., Huyet, J., Pinon, G.M., Rochel, M., Mayer, C., and Rafestin-Oblin, M.E. (2005). Crystal structure of a mutant mineralocorticoid receptor responsible for hypertension. Nat. Struct. Mol. Biol. *12*, 554–555.

Fang, L., Ricketson, D., Getubig, L., and Darimont, B. (2006). Unliganded and hormone-bound glucocorticoid receptors interact with distinct hydrophobic sites in the Hsp90 C-terminal domain. Proc. Natl. Acad. Sci. USA *103*, 18487–18492.

Grad, I., and Picard, D. (2007). The glucocorticoid responses are shaped by molecular chaperones. Mol. Cell Endocrinol. *275*, 2–12.

Gravez, B., Tarjus, A., and Jaisser, F. (2013). Mineralocorticoid receptor and cardiac arrhythmia. Clin. Exp. Pharmacol. Physiol. *40*, 910–915.

Gronemeyer, H., Gustafsson, J.A., and Laudet, V. (2004). Principles for modulation of the nuclear receptor superfamily. Nat. Rev. Drug Discov. *3*, 950–964.

Gunnarsson, A., Snijder, A., Hicks, J., Gunnarsson, J., Höök, F., and Geschwindner, S. (2015). Drug discovery at the single molecule level: inhibition-in-solution assay of membrane-reconstituted β-secretase using single-molecule imaging. Anal. Chem. *87*, 4100–4103.

Hasui, T., Matsunaga, N., Ora, T., Ohyabu, N., Nishigaki, N., Imura, Y., Igata, Y., Matsui, H., Motoyaji, T., Tanaka, T., et al. (2011). Identification of benzoxazin-3-one derivatives as novel, potent, and selective nonsteroidal mineralocorticoid receptor antagonists. J. Med. Chem. *54*, 8616–8631.

Hughes, T.S., Chalmers, M.J., Novick, S., Kuruvilla, D.S., Chang, M.R., Kamenecak, T.M., Rance, M., Johnson, B.A., Burris, T.P., Griffin, P.R., et al. (2012). Ligand and receptor dynamics contribute to the mechanism of graded PPARg agonism. Structure *20*, 139–150.

Kohn, J.A., Deshpande, K., and Ortlund, E.A. (2012). Deciphering modern glucocorticoid cross-pharmacology using ancestral corticosteroid receptors. J. Biol. Chem. *287*, 16267–16275.

Kotev, M., Lecina, D., Tarragó, T., Giralt, E., and Guallar, V. (2015). Unveiling prolyl oligopeptidase ligand migration by comprehensive computational techniques. Biophys. J. *108*, 116–125.

Larkin, M.A., Blackshields, G., Brown, N.P., Chenna, R., McGettigan, P.A., McWilliam, H., Valentin, F., Wallace, I.M., Wilm, A., Lopez, R., et al. (2007). Clustal W and Clustal X version 2.0. Bioinformatics *23*, 2947–2948.

Li, Y., Suino, K., Daugherty, J., and Xu, H.E. (2005). Structural and biochemical mechanisms for the specificity of hormone binding and coactivator assembly by mineralocorticoid receptor. Mol. Cell *19*, 367–380.

Madhavi Sastry, G., Adzhigirey, M., Day, T., Annabhimoju, R., and Sherman, W. (2013). Protein and ligand preparation: parameters, protocols, and influence on virtual screening enrichments. J. Comput. Aided Mol. Des. *27*, 221–234.

Mangelsdorf, D.J., Thummel, C., Beato, M., Herrlich, P., Schütz, G., Umesono, K., Blumberg, B., Kastner, P., Mark, M., Chambon, P., and Evans, R.M. (1995). The nuclear receptor superfamily: the second decade. Cell *83*, 835–839.

Matias, P.M., Donner, P., Coelho, R., Thomaz, M., Peixoto, C., Macedo, S., Otto, N., Joschko, S., Scholz, P., Wegg, A., et al. (2000). Structural evidence for ligand specificity in the binding domain of the human androgen receptor. Implications for pathogenic gene mutations. J. Biol. Chem. *275*, 26164–26171.

Moras, D., and Gronemeyer, H. (1998). The nuclear receptor ligand-binding domain: structure and function. Curr. Opin. Cell Biol. *10*, 384–391.

Nettles, K.W., Bruning, J.B., Gil, G., O'Neill, E.E., Nowak, J., Guo, Y., Kim, Y., DeSombre, E.R., Dilis, R., Hanson, R.N., et al. (2007). Structural plasticity in the oestrogen receptor ligand-binding domain. EMBO Rep. *8*, 563–568.

Ortlund, E.A., Bridgham, J.T., Redinbo, M.R., and Thornton, J.W. (2007). Crystal structure of an ancient protein: evolution by conformational epistasis. Science *317*, 1544–1548.

Osz, J., Brélivet, Y., Peluso-Iltis, C., Cura, V., Eiler, S., Ruff, M., Bourguet, W., Rochel, N., and Moras, D. (2012). Structural basis for a molecular allosteric control mechanism of cofactor binding to nuclear receptors. Proc. Natl. Acad. Sci. USA *109*, E588–E594.

Perrière, G., and Gouy, M. (1996). WWW-Query: an on-line retrieval system for biological sequence banks. Biochimie *78*, 364–369.

Pfaff, S.J., and Fletterick, R.J. (2010). Hormone binding and co-regulator binding to the glucocorticoid receptor are allosterically coupled. J. Biol. Chem. *285*, 15256–15267.

Ricketson, D., Hostick, U., Fang, L., Yamamoto, K.R., and Darimont, B.D. (2007). A conformational switch in the ligand-binding domain regulates the dependence of the glucocorticoid receptor on Hsp90. Mol. Biol. *368*, 729–741.

Rupprecht, R., Reul, J.M.H.M., van Steensel, B., Spengler, D., Söder, M., Berning, B., Holsboer, F., and Damm, K. (1993). Pharmacological and functional characterization of human mineralocorticoid and glucocorticoid receptor ligands. Eur. J. Pharmacol. *247*, 145–154.

Schrödinger. (2013). Release 2013-1: MacroModel, Version 10.0 (Schrödinger, LLC).

Shelley, M., Bennett, C., Nathan, D., and Sartor, O. (2008). Non-steroidal anti-androgen use as part of combined androgen blockade therapy for metastatic or locally advanced prostate cancer: a review of the evidence on efficacy and toxicity. In Cancer metastasis-biology and treatment, R.J. Ablin and M.D. Mason, eds. (Springer Science and Business Media), pp. 283–307.

Shibata, S., Rinehart, J., Zhang, J., Moeckel, G., Castañeda-Bueno, M., Stiegler, A.L., Boggon, T.J., Gamba, G., and Lifton, R.P. (2013). Mineralocorticoid receptor phosphorylation regulates ligand binding and renal response to volume depletion and hyperkalemia. Cell Metab. *18*, 660–671.

Sitruk-Ware, R., and Nath, A. (2010). The use of newer progestins for contraception. Contraception *82*, 410–417.

Soisson, S.M., Parthasarathy, G., Adams, A.D., Sahoo, S., Sitlani, A., Sparrow, C., Cui, J., and Becker, J.W. (2008). Identification of a potent synthetic FXR agonist with an unexpected mode of binding and activation. Proc. Natl. Acad. Sci. USA *105*, 5337–5342.

Sonoda, M.T., Martínez, L., Webb, P., Skaf, M.S., and Polikarpov, I. (2008). Ligand dissociation from estrogen receptor is mediated by receptor dimerization: evidence from molecular dynamics simulations. Mol. Endocrinol. *22*, 1565–1578.

Takahashi, R., Gil, V.A., and Guallar, V. (2014). Monte Carlo free ligand diffusion with Markov state model analysis and absolute binding free energy calculations. J. Chem. Theor. Comput. *10*, 282–288.

Waterhouse, R.M., Tegenfeldt, F., Li, J., Zdobnov, E.M., and Kriventseva, E.V. (2013). OrthoDB: a hierarchical catalog of animal, fungal and bacterial orthologs. Nucleic Acids Res. *41*, D358–D365.

Williams, S.P., and Sigler, P.B. (1998). Atomic structure of progesterone complexed with its receptor. Nature *393*, 392–396.

Yen, P.M. (2001). Physiological and molecular basis of thyroid hormone action. Physiol. Rev. *81*, 1097–1142.

